REPORT DOCUMENTATION PAGE

Form Approved
OMB No. 0704-0188

1. REPORT DATE *(DD-MM-YYYY)*	**2. REPORT TYPE**	**3. DATES COVERED** *(From - To)*
01-12-2007	Journal Article	1 Dec 07 – 1 Dec 07

4. TITLE AND SUBTITLE

Advances in SiGeSn Technology

5a. CONTRACT NUMBER
IN-HOUSE

5b. GRANT NUMBER

5c. PROGRAM ELEMENT NUMBER
61102F

6. AUTHOR(S)

Richard Soref, *John Kouvetakis, *John Tolle, **Jose Menendez, **Vijay D'Costa

5d. PROJECT NUMBER
2305

5e. TASK NUMBER
HC

5f. WORK UNIT NUMBER
01

7. PERFORMING ORGANIZATION NAME(S) AND ADDRESS(ES)
Optoelectronic Technology Branch, 80 Scott Drive, Hanscom AFB, MA 01731-2909; *Department of Chemistry and Biochemistry, Arizona State University, Tempe AZ 85287; **Department of Physics and Astronomy, Arizona State University, Tempe AZ 85287

8. PERFORMING ORGANIZATION REPORT

9. SPONSORING / MONITORING AGENCY NAME(S) AND ADDRESS(ES)
Electromagnetics Technology Division Source Code: 437890
Sensors Directorate
Air Force Research Laboratory
80 Scott Drive
Hanscom AFB MA 01731-2909

10. SPONSOR/MONITOR'S ACRONYM(S)
AFRL-RY-HS

11. SPONSOR/MONITOR'S REPORT NUMBER(S)
AFRL-RY-HS-TP-2008-0013

12. DISTRIBUTION / AVAILABILITY STATEMENT
DISTRIBUTION A: APPROVED FOR PUBLIC RELEASE; DISTRIBUTION UNLIMITED.

13. SUPPLEMENTARY NOTES
The U. S. Government is joint author of this work and has the right to use, modify, reproduce, release, perform, display, or disclose the work. Published in Journal of Materials Research, vol. 22, pp. 3281-3291, December 2007. Cleared for Public Release by ESC/PA number: ESC-07-0583.

14. ABSTRACT
We recently reported the CVD growth of binary $Ge_{1-y}Sn_y$ and ternary $Ge_{1-y}Si_xSn_y$ alloys directly on Si wafers using SnD_4, Ge_2H_6 (di-germane), SiH_3GeH_3, and $(GeH_3)_2SiH_2$ sources. $Ge_{1-y}Sn_y$ is an intriguing infrared material that undergoes an indirect-to-direct bandgap transition for $y < 0.1$. In addition, we have found that $Ge_{1-y}Sn_y$ layers have ideal properties as templates for the subsequent deposition of other semiconductors: (a) they are strain-relaxed and have low threading-defect densities (10^5 cm^{-2}) even for films thinner than 1 μm; (b) their low growth temperatures between 250°C and 350°C are compatible with selective growth, and the films possess the necessary thermal stability for conventional semiconductor processing (up to 750°C depending on composition); (c) they exhibit tunable lattice constants between 5.65 Å and at least 5.8 Å, matching InGaAs and related III-V systems; (d) their surfaces are extremely flat; (e) they grow selectively on Si and not on SiO_2; and (f) the film surface can be prepared by simple chemical cleaning for subsequent *ex-situ* epitaxy. The incorporation of Sn lowers the absorption edges of Ge. Therefore, $Ge_{1-y}Sn_y$ is attractive for detector and photovoltaic applications that require band gaps lower than that of Ge. Spectroscopic ellipsometry and photoreflectance experiments show that the direct band gap is halved for as little as $y = 0.15$. Studies of a $Ge_{0.98}Sn_{0.02}$ sample yield an absorption coefficient of 3500 cm^{-1}at 1675 nm (0.74 eV). Thus infrared detectors based on $Ge_{0.98}Sn_{0.02}$ could easily cover the U-(1565 nm-1625 nm), L-(1565 nm-1625 nm), and C-(1530 nm-1565 nm) telecomm bands. Photoluminescence studies show band gap emission on thin GeSn layers sandwiched between higher bandgap SiGeSn barriers. We have made advances in p and n doping of GeSn and present results on electrical characterizations.

15. SUBJECT TERMS
CVD growth, band gap emission

16. SECURITY CLASSIFICATION OF:			**17.LIMITATION OF ABSTRACT**	**18.NUMBER OF PAGES**	**19a. NAME OF RESPONSIBLE PERSON**
a. REPORT	**b. ABSTRACT**	**c. THIS PAGE**			**19b. TELEPHONE NUMBER** *(include area code)*
Unclassified	Unclassified	Unclassified	SAR	16	Richard Soref N/A

Standard Form 298 (Rev. 8-98)
Prescribed by ANSI Std. Z39.18

Journal of Materials Research, vol. 22, pp. 3281-3291, December 2007

Advances in SiGeSn Technology

Richard A. Soref

Sensors Directorate, Air Force Research Laboratory,
Hanscom Air Force Base, MA 01731

J. Kouvetakis and John Tolle

Department of Chemistry and Biochemistry, Arizona Sate University,
Tempe AZ 85287

J. Menendez and Vijay D'Costa

Department of Physics and Astronomy, Arizona Sate University,
Tempe AZ 85287

ABSTRACT

We recently reported the CVD growth of binary $Ge_{1-y}Sn_y$ and ternary $Ge_{1-y}Si_xSn_y$ alloys directly on Si wafers using SnD_4, Ge_2H_6 (di-germane), SiH_3GeH_3, and $(GeH_3)_2SiH_2$ sources. $Ge_{1-y}Sn_y$ is an intriguing infrared material that undergoes an indirect-to-direct bandgap transition for $y < 0.1$. In addition, we have found that $Ge_{1-y}Sn_y$ layers have ideal properties as templates for the subsequent deposition of other semiconductors: (a) they are strain-relaxed and have low threading-defect densities (10^5 cm^{-2}) even for films thinner than 1 μm; (b) their low growth temperatures between 250°C and 350°C are compatible with selective growth, and the films possess the necessary thermal stability for conventional semiconductor processing (up to 750°C depending on composition); (c) they exhibit tunable lattice constants between 5.65 Å and at least 5.8 Å, matching InGaAs and related III-V systems; (d) their surfaces are extremely flat; (e) they grow selectively on Si and not on SiO_2; and (f) the film surface can be prepared by simple chemical cleaning for subsequent *ex-situ* epitaxy. The incorporation of Sn lowers the absorption edges of Ge. Therefore, $Ge_{1-y}Sn_y$ is attractive for detector and photovoltaic applications that require band gaps lower than that of Ge. Spectroscopic ellipsometry and photoreflectance experiments show that the direct band gap is halved for as little as $y = 0.15$. Studies of a $Ge_{0.98}Sn_{0.02}$ sample yield an absorption coefficient of 3500 cm^{-1}at 1675 nm (0.74 eV). Thus infrared detectors based on $Ge_{0.98}Sn_{0.02}$ could easily cover the U-(1565 nm-1625 nm), L-(1565 nm-1625 nm), and C-(1530 nm-1565 nm) telecomm bands. Photoluminescence studies show band gap emission on thin GeSn layers sandwiched between higher bandgap SiGeSn barriers. We have made advances in p and n doping of GeSn and present results on electrical characterizations. Hall measurements reveal mobilities as high as of 600 cm^2/V-s and background p-dopants concentrations in the $10^{-6}/cm^3$ range for samples with nominal composition and thickness of $Ge_{0.98}Sn_{0.02}$ and ~ 500 nm, respectively. GeSn also has application in band-to-band laser heterodiodes. The ternary system $Ge_{1-x-y}Si_xSn_y$ grows on $Ge_{1-y}Sn_y$-buffered

Si. It represents the first practical group-IV ternary alloy, since C can only be incorporated in minute amounts to the Ge-Si network. The most significant feature of $Ge_{1-x-y}Si_xSn_y$ is the possibility of independent adjustment of lattice constant and band gap. For the same value of the lattice constant one can obtain band gaps differing by more than 0.2 eV, even if the Sn-concentration is limited to the range $y < 0.2$. This property can be used to develop a variety of novel devices, from multicolor detectors to multiple junction photovoltaic cells. A linear interpolation of band gaps lattice constants between Si, Ge and α-Sn shows that it is possible to obtain SiGeSn with a band gap and a lattice constant larger than that of Ge. We shall use this feature to make a tensile-strained Ge-on-SiGeSn telecomm detector with improved performance. To date record high tensile strain (0.40%) has been achieved in Ge layers grown on GeSn buffered Si where the strain is systematically tuned by adjusting the lattice constant in the buffer. A tensile-strain-induced direct gap of Ge can be used also for laser diodes and electroptical modulators.

INTRODUCTION

High-quality strain-relaxed buffer layers of GeSn and SiGeSn have been grown upon a silicon substrate at Arizona State University. This heteroepitaxy has added momentum to the emergence of silicon-based photonics (also known as group IV photonics). Recent ASU work proves that the buffer layer is an excellent template for the subsequent growth of high-quality GeSn/Ge, SiGeSn/Ge, SiGeSn/GeSn and SiSn/GeSn heterostructures, as well as III-V compound semiconductors. The purpose of this paper is to report recent advances in: (1) novel heteroepitaxy and strained-layer engineering directly on silicon, (2) band-structure predictions for heterostructures including quantum well stacks, (3) design of photonic devices, including experimental results on photoemission and luminescence. The GeSn technology described here [1-11] is intended ultimately for application in silicon-based optoelectronics. This technology is expected to be fully compatible, foundry compatible, with CMOS electronics. Of course, it is possible to make discrete, stand-alone GeSn/Ge photonic components, but our main thrust is to create active, waveguided GeSn photonic components for use in photonic integrated circuits (PICs) and optoelectronic integrated circuits (OEICs). The PICs offer "seamless" monolithic integration of photonic components, while OEICs give seamless integration of electronics and photonics in the same Si chip. An important benefit of such ICs is that they can be designed for operation at any wavelength within the mid, far, and very far infrared (THz) range.

The future of GeSn photonics is ripe with possibilities. If we examine the designs for electrically controlled-or-driven GeSn photonic devices, we find that there are two kinds: (A) conduction-to-valence *band-to-band* devices for the 1.5 to 8 μm wavelength range, (B) conduction- or valence-*intersubband* devices for the 8 to 200 μm wavelength range. Type A can use layers that are 100s of nm thick, or quantum confined layers less than 10 nm thick; whereas Type B will employ MQWs-- as in quantum cascade lasers and quantum well infrared photodetectors. The longer the wavelength of operation, the more likely it is that cryo cooling will be required. The principal devices that we are seeking in this GeSn technology are: laser diodes, infrared amplifiers, photodetectors, electrooptical modulators and EO routing switches. The evidence so far suggests that each of these devices is feasible, although major work remains to prove that assertion.

In 2006, the Air Force Office of Scientific Research launched a MURI on electrically pumped silicon-based lasers. Two teams, one led by the Massachusetts Institute of Technology, and the other by Arizona State University, are investigating the lasers. The MIT team has two approaches, one of which relies upon the intrinsic gain in tensile Ge within an Si/Ge/Si heterostructure. The ASU team will investigate band-to-band lasing and intersubband quantum-cascade lasing (QCL) in the SiGeSn/Ge system. MIT uses the thermal-expansion mismatch between Ge and Si to attain tensile-strained Ge. For their Ge-on-Si growth at 800 ^{o}C, a maximum tensile strain of 0.27 % is theoretically possible, and MIT has observed 0.20 % experimentally.
ASU employs tensile-strained Ge grown upon GeSn or SiGeSn buffered Si (100) in which the strain is adjusted by tuning the lattice constant of the underlying buffer. Their extensive theoretical studies show that the Ge gap becomes direct at 2% strain. For strain less than 2 %, the gap of tensile Ge is "almost direct". ASU has conducted Ge CVD growth in the 350-400 ^{o}C CMOS compatible range to produce record-high strain in Ge/GeSn/Si heterostructures as described below using a specially developed technique based on purpose built molecular sources.

THEORY, EXPERIMENT AND BACKGROUND

SiGeSn/Ge heterostructures grown directly upon silicon provide new photonic capabilities within the photonic layer of a Si optelectronic chip. These heterodevices can overcome limitations imposed by the indirect bandgap of Si because a direct bandgap can be attained in the alloy layers (and in Ge itself) by means of strain engineering and alloy- composition engineering. Such directness opens up a host of device possibilities across the wide infrared range.

(a) Synthesis and optical properties of GeSn alloys: The ASU $Ge_{1-y}Sn_y$ alloys are grown by a specially developed CVD method [1]. The combination of SnD_4 with high-purity H_2 (15-20%) remains remarkably stable at 22°C for extended time periods. This formulation provides the simplest possible CVD source of Sn atoms for the growth of novel Sn containing systems. Depositions are conducted in a UHV-CVD reactor on Si(100) wafers. Growth temperatures between 250°C and 350°C produce thick films (50-500 nm) with Sn concentrations up to 20%, as measured by RBS (Fig. 1). $Ge_{1-y}Sn_y$ films grow nearly relaxed on Si, as evidenced by high resolution XRD. The surfaces are continuous and atomically flat (AFM-RMS 0.5 -1.0 nm). The XTEM micrographs (Fig. 1) reveal extremely low threading dislocation densities in the range of 10^5 cm^{-2}. The predominant defects accommodating the large misfit between the alloys and the Si substrate are Lomer edge dislocations at the interface. These are parallel to the interface plane and do not degrade the film quality. Further XTEM and SIMS measurements show no evidence of diffusion, clustering, segregation, or spiking that is observed in other materials deposited on Si. Thus $Ge_{1-y}Sn_y$ appears to be viable from a contamination and device perspective to be introduced into CMOS fabrication for integrated optoelectronics.

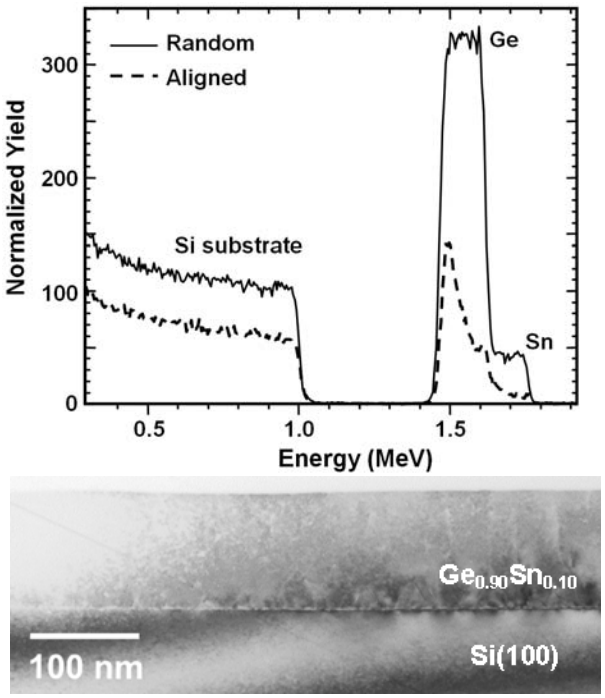

Figure 1. (top): RBS random (solid trace) and aligned (dotted line) spectra of a 250 nm $Ge_{0.94}Sn_{0.06}$ film grown on Si(100). The ratio of the aligned-versus-random-peak heights is the same for both elements, indicating complete substitutionality of Sn in the structure. **(bottom):** XTEM bright field image of an $Ge_{0.90}Sn_{0.10}$ showing a defect free layer.

We believe that this development represents a breakthrough in Si-based manufacturing technology because these $Ge_{1-y}Sn_y$ layers have ideal properties as templates for the subsequent deposition of other semiconductors [2,3]: (a) they are strain-relaxed and have low threading defect densities (10^5 cm^{-2}) even for films thinner than 1 μm; (b) their low growth temperatures are compatible with selective growth, and the films possess the necessary thermal stability for conventional semiconductor processing (up to 750°C depending on composition); (c) they exhibit tunable

lattice constants between 5.65 Å and at least 5.8 Å, well within the range of virtually all III-V and II-VI systems; (d) their flat surfaces provide an ideal platform for subsequent growth; (e) they grow selectively on Si and not on SiO_2; and (f) the film surface can be prepared by simple chemical cleaning for subsequent *ex-situ* epitaxy.

In addition to their demonstrated value as versatile buffer layers (see below) for growth on Si, the $Ge_{1-y}Sn_y$ alloys possess intriguing properties that make them suitable as active materials in optoelectronic applications, including detectors, photovoltaics, and lasers. The incorporation of Sn lowers the direct and indirect absorption edges of Ge. Therefore, this material is attractive for detector and photovoltaic applications that require band gaps lower than that of Ge. One of the drawbacks of Si-based photodetectors is that they cannot cover the extended optical communication wavelength windows between 1.26 –1.67 μm. In fact, Ge barely reaches the 1.55 μm range. For this particular application, even a small amount of Sn would suffice. The potential of $Ge_{1-y}Sn_y$ for laser devices stems from the prediction that this alloy system should undergo an indirect-to-direct gap transition for $y = 0.2$. We have measured the compositional dependence of the direct band gap for the limited compositional range produced to date. These experiments demonstrated a dramatic band gap reduction of the Ge-like optical transitions (the first direct gap E_0, the split-off $E_0+\Delta_0$ gap, and the higher-energy E_1, $E_1+\Delta_1$, E_0' and E_2 structures) as a function of the Sn concentration [4,5]. We find that with only 14 at. % Sn the direct band gap is halved relative to its value in pure Ge [4]. This measured compositional dependence deviates both from prior theoretical predictions and from a simple linear interpolation between Ge and α-Sn.

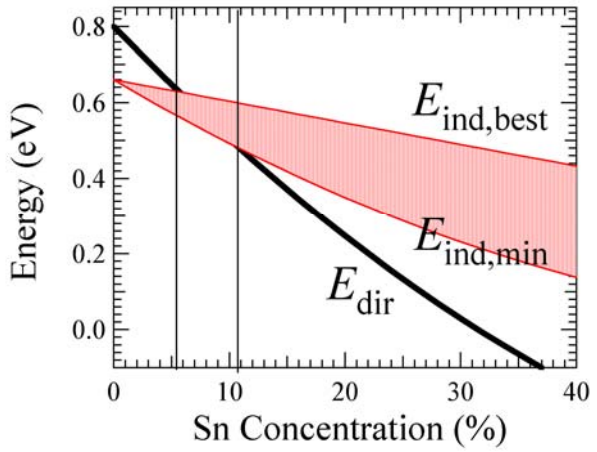

Figure 2. Bandgap energies of an unstrained $Ge_{1-y}Sn_y$. The two plots of the indirect gap are based on estimates that are discussed in detail in reference.

Our direct measurements of the band structure indicate that the indirect/direct crossover should occurs for Sn concentrations of $y < 0.1$ as shown in Fig. 2 [5]. This should make it much easier to reach the direct-gap phase suggesting that PL should be observable in these materials for modest Sn concentrations. It is well known that light emission in group-IV materials is extremely sensitive to defects and impurities. The goal is therefore to further improve the microstructure of GeSn in order to promote light emission. One strategy, pursued recently, is to form multilayer stacks based on lattice matched SiGeSn/GeSn/SiGeSn structures grown directly on GeSn buffered Si(100) wafers. In this approach the active GeSn layer is ensconced within the higher band gap SiGeSn barrier layers. We find that the defects in these samples are confined to the Si(100) interface while the remainder of the stack remains virtually defect free. This geometry is designed to keep the defects away from the carriers in the active material. In addition the closer proximity of the electron hole pairs increases their recombination rate. Fig. 3(a) demonstrates a realization of this design experimentally by showing Z-contrast micrographs of a single SiGeSn/GeSn/SiGeSn unit grown on GeSn buffered Si substrate. The layers display coherent, atomically abrupt interfaces and a perfectly uniform thickness as confirmed by the atomic level image of the GeSn active

layer region. This level of microstructural control, normally only achievable by MBE, is remarkable in a CVD grown sample.

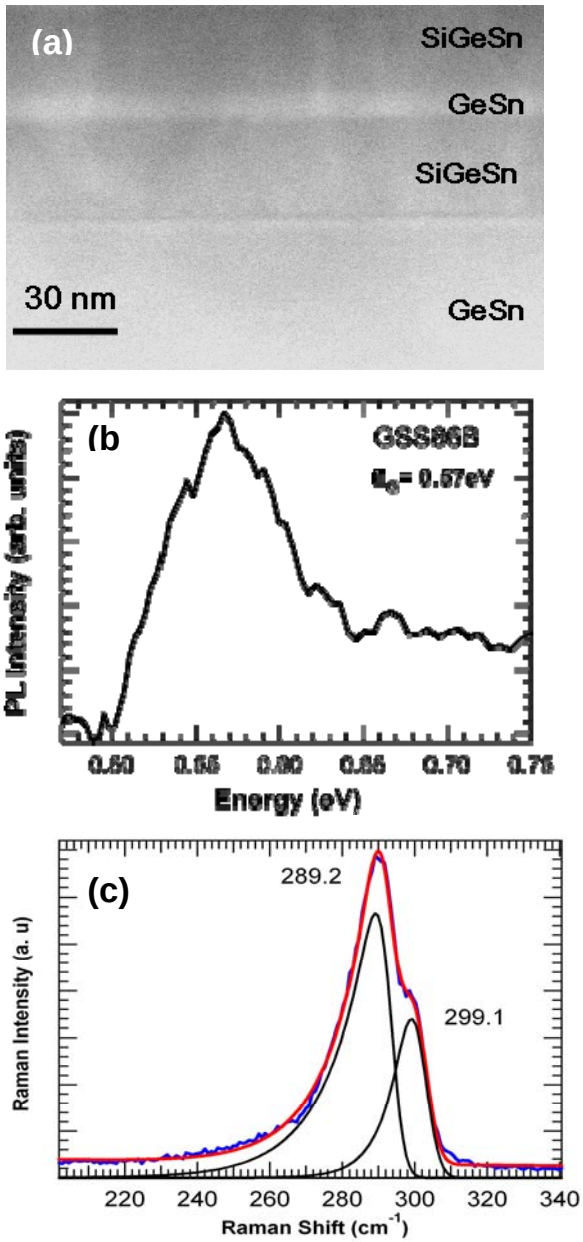

Figure 3: (a) Z-contrast XTEM image of a single SiGeSn/GeSn/GeSiSn stack. **(b)** PL of a GeSn quantum well. **(c)** Typical Raman spectrum of a light emitting layer structure.

Optical measurements showed that these high quality samples display distinct PL peaks for the first time near the expected band gap wavelength. Fig. 3(b) shows the PL signal from a GeSn sample with ~ 2.5 % Sn as measured by RBS. Note that the signal is relatively weak due to the indirect nature of the $Ge_{0.975}Sn_{0.025}$ band gap and the small sample volume, but it has been confirmed in power dependence studies. Furthermore, it is found to be uniform across the sample and other samples with 2-3% Sn content display similar band gap emission.

Since errors in RBS determinations can be large in multilayer systems sharing the same atomic species, we developed a Raman scattering method to confirm the RBS compositional results. We performed Raman experiments on many single $Ge_{1-x-y}Si_xSn_y$ and $Ge_{1-y}Sn_y$ layers and calibrated the Raman frequencies as a function of composition and strain. In Fig. 1(c) we show the spectrum of a simple SiGeSn/GeSn/SiGeSn/GeSn(buffer)Si(100) heterostructure. The high-energy peak corresponds to the GeSn layer, and from its frequency the Sn concentration is calculated to be 2.5 %. The main peak corresponds to the GeSiSn barrier layers. It should have a frequency of 288.3 cm^{-1} based on the measured RBS concentrations which is close to the experimental value of 289.2 cm^{-1}.

Notice that the PL energy is slightly below the expected position of the indirect edge in $Ge_{0.975}Sn_{0.025}$. This is probably due to the well-known Stokes shift of the PL with respect to the absorption in alloy semiconductors. The absorption edge is expected to be approximately 60 meV higher.

The results shown here demonstrate the maturity reached by the materials science effort in that we have achieved the required control of composition, thicknesses and defect mitigation in multilayer stacks. The stack sequence shown in Fig. 2(a) can be repeated over several periods as needed. Thus the project is ready to move into a systematic study of composition vs. PL

measurements. The goal is to produce the direct band gap emission expected for Sn compositions in the range of 6-10 %.

(b) Doping strategies and electrical measurements: Hall and IR ellipsometry measurements of $Ge_{1-y}Sn_y$ indicate that as-grown material is *p*-type, with hole concentrations in the 10^{16} cm^{-3} range. This background doping is found to be due to defects in the as-grown material and can be considerably reduced upon rapid thermal annealing of the samples in the range of 600-700 ^oC. This occurs with a simultaneous increase in mobility, suggesting that the thermal treatment is truly removing the acceptor defects rather than creating compensating donor defects. Electrically active defects and unintentional dopants increase the possibility of undesirable dark currents in these materials.

The measured hole motilities of our samples were found to be closely dependent on the annealing temperature, the sample thickness and the specific growth conditions. To date mobility values as high as 600 cm^2/V-s have been obtained for samples with composition of $Ge_{0.98}Sn_{0.02}$ and nominal thicknesses of 450-500 nm. These materials were deposited directly on Si at 350 ^oC at a rate of ~ 8 nm /min utilizing an excess of elemental hydrogen in the reaction mixture. A post growth annealing step was conducted at 650 C^o for 30 seconds which resulted in a substantial reduction in the number of penetrating threading defects without compromising the atomically flat surface morphology of the as grown material. The corresponding carrier concentration and resistivity values of the annealed $Ge_{0.98}Sn_{0.02}$ samples were measured to be $5.6x10^{16}/cm^3$ and 0.265 Ω.cm, respectively. The hole mobilties of thinner samples, 250-300 nm, were significantly lower indicating that the interface defects due to the lattice mismatch act as scattering centers limiting the transport properties of the material.

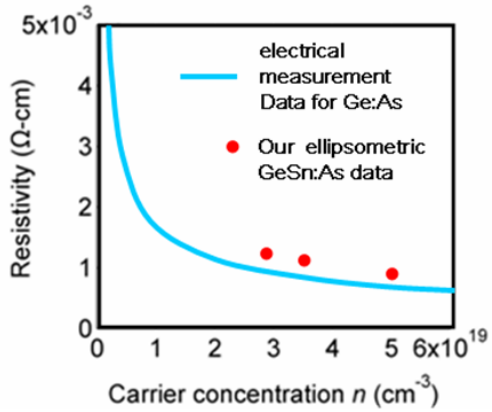

Figure 4. Concentration dependence of resistivity for three GeSn:As samples. Blue line is the electrical data from standard As-doped Ge samples.

Critical for the development of GeSn based devices is the ability to create *n* and *p*-type layers. We have initiated work in this area and found that n-doping cannot be achieved via AsH_3 due to incompatibilities with the low growth temperatures required for GeSn. We therefore developed an alternative chemical approach to incorporate high concentrations of active *n*-dopant atoms into group-IV semiconductors without clustering or segregation. This involves the use of carbon-free single-source inorganic hydrides which are ideal for low temperature, high efficiency doping applications. Controlled substitution of As is made possible by the use of $As(GeH_3)_3$, which furnishes structurally and chemically compatible $AsGe_3$ molecular cores [6].

Proof-of-principle was demonstrated by the growth of $Ge_{0.97}Sn_{0.03}(As)$ films with As concentration ~ 3×10^{19} atoms/cm^3. TEM, SIMS, AFM, RBS, HR-XRD characterizations showed defect- and strain free interfacial morphology, excellent compositional uniformity, very low surface roughness, and exceptional crystallinity. A contactless ellipsometric technique was used to determine electrical properties and demonstrated high carrier concentrations in $As(GeH_3)_3$–doped $Ge_{1-y}Sn_y$. An example is shown in Fig. 4 where the results of this new technique are

compared with conventional electrical determinations for pure Ge (blue line; ellipsometric measurements from pure Ge also fall on this line) [6]. Typical values for the resistivity and relaxation time are $\rho_0 = 0.0124$ Ωcm and $\tau = 1.14\times10^{-14}$ s, while an effective mass $m^* = 0.094\ m_e$ (average of the *L*-valley and the Γ-valley masses) was found to bring ellipsometric and SIMS measurements of the concentration data into agreement. Fig. 4 also shows that for the same carrier concentration, the resistivity of the $Ge_{1-y}Sn_y$ layers is only slightly higher than that of Ge. This remarkable result shows that alloy scattering does not play a significant role in transport phenomena in $Ge_{1-y}Sn_y$ alloys. Alloy scattering in $Si_{1-x}Ge_x$ is small enough to allow high performance electronic devices. However, alloy scattering in $Ge_{1-y}Sn_y$ was expected to be far more dramatic due to the much larger mismatch in lattice constants (14% vs. 4% in $Si_{1-x}Ge_x$). The fact that alloy scattering is minimal is very encouraging for the development of $Ge_{1-y}Sn_y$ devices.

(c) Synthesis and optical properties of GeSiSn ternary alloys: Recently we have demonstrated the growth of single-phase, monocrystalline $Ge_{1-x-y}Si_xSn_y$ alloys that possess a variable and controllable range of compositions and exhibit lattice constants above and below that of bulk Ge [7]. These ternaries are grown on Si(100) via $Ge_{1-y}Sn_y$ buffers, as illustrated by TEM data in Fig. 5. The growth of $Ge_{1-x-y}Si_xSn_y$ is accomplished by using the SiH_3GeH_3, $(GeH_3)_2SiH_2$, and $(GeH_3)_3SiH$ hydrides as the source of the Si and Ge atoms. These are the key precursors that furnish building blocks of specifically tailored elemental contents and possess the necessary reactivity to readily form the desired metastable structures and concentrations at low temperatures of 300-350 °C. For example, $(GeH_3)_2SiH_2$ reacts readily with SnD_4 at 350 °C to yield films with a ratio of 2(Ge):Si precisely matching that of the corresponding precursor. This illustrates that the starting material largely determines the final composition of the film. In practice we find that this approach affords compositional control that is impossible to achieve using either conventional CVD based on simple silanes and germanes, or by MBE using solid sources.

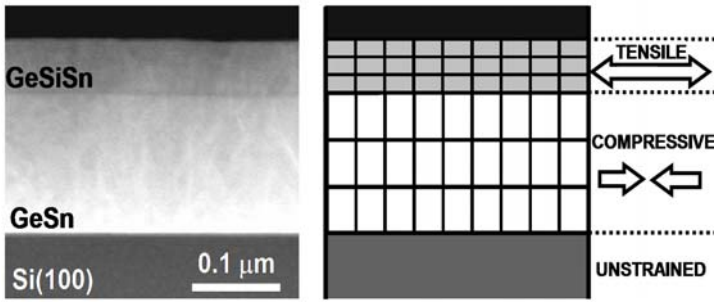

Figure 5. Left: XTEM, Z-contrast image of a tensile strained $Ge_{0.64}Si_{0.32}Sn_{0.04}$ epilayer (light contrast) and a compressively strained $Ge_{0.97}Sn_{0.03}$ buffer. The film surface is flat and the both layers are highly uniform and perfectly coherent. Right: schematic of the heterostructure illustrating the relative strain states of the epilayer and buffer when they share a common parallel lattice constant (see Ref. 8)

We have been able to grow a host of device-quality $Ge_{1-y}Sn_y/Ge_{1-x-y}Si_xSn_y$ samples. A detailed x-ray analysis shows that the $Ge_{1-x-y}Si_xSn_y/Ge_{1-y}Sn_y$ stack achieves a final strain state that minimizes the bilayer elastic energy, as if the films were decoupled from the substrate [8] (Fig 5). Accordingly, we can obtain strained (tensile and compressive) as well as relaxed and lattice-matched $Ge_{1-x-y}Si_xSn_y$ films on suitable $Ge_{1-y}Sn_y$ buffers. From the point of view of possible applications in optoelectronics, the most significant feature of the $Ge_{1-x-y}Si_xSn_y$ ternary system is the possibility of independent adjustment of lattice constant and band gap. In principle a wide range of band gaps can be achieved by adjusting the Si/Sn ratio in the alloy. In fact for the same

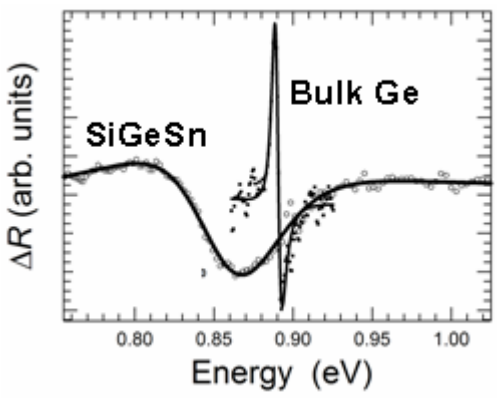

Figure 6. Photoreflectance signal from a $Ge_{1-x-y}Si_xSn_y$ layer in the vicinity of the direct gap E_0. For comparison, the same signal for pure a Ge wafer is also displayed.

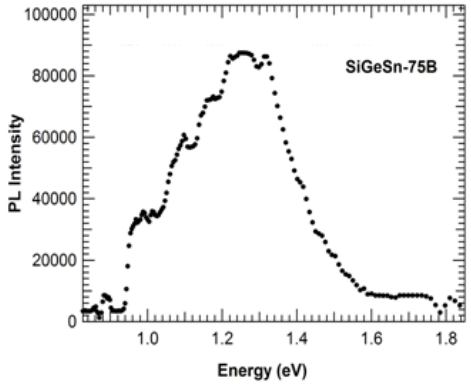

Figure 7. Band gap PL form a SiGeSn layer with 7% Sn.

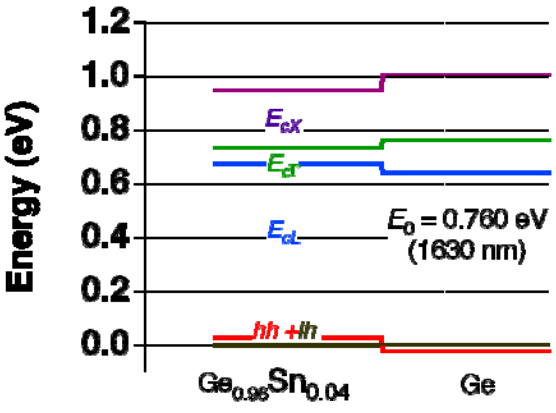

Figure 7. Predicted band edge energies and band alignment of partially strained Ge

value of the lattice constant one can obtain band gaps differing by more than 0.2 eV, even if the Sn-concentration is limited to the range $y < 0.2$. The continuum of band gaps for a fixed lattice constant can be used to develop a variety of devices from multicolor detectors to multiple junction photovoltaic cells.

The initial studies of the optical properties of $Ge_{1-x-y}Si_xSn_y$ alloys have been conducted using IR and UV/visible ellipsometry. In all cases, the $Ge_{1-x-y}Si_xSn_y$ critical point transition energies (E_1, $E_1+\Delta_1$, E_0' and E_2) show a negative deviation relative to the weighted average of the corresponding energies in elemental Si, Ge and α–Sn. These deviations from "Vegard's law" can be characterized by quadratic terms of the form $-b^{AB}x^Ax^B$ (where the bowing coefficients b^{AB} = [b^{SiGe}, b^{GeSn}, b^{SiSn}] and x is the concentration). The results suggest that these bowing coefficients follow a simple scaling behavior with the electronegativity and size difference between Si, Ge, and α-Sn [9]. This is remarkable from a fundamental viewpoint and very useful from a practical perspective. If all important transitions follow a similar trend, it should be much easier to develop two-dimensional maps of band gap values as a function of the compositional variables x and y. The critically important direct gap E_0 is difficult to measure with ellipsometry, but we have preliminary photoreflectance (PR) data suggesting that this technique is suitable for the detection of E_0. Fig. 6 shows the PR spectrum recorded at 10 K from a Ge wafer and a GeSiSn film grown on Si(100) via a GeSn buffer. Note that the direct band gap (E_0) for the film is close to 0.80 eV, which is well within the desired communication wavelength range. The SiGeSn system has therefore an intriguing potential for applications in this area and represents an attractive alternative to GeSn and SiGe for the fabrication of Si-based photonic devices. Fig. 7 shows an example of a PL spectrum from a sample containing 7% Sn on GeSn tentatively assigned to the lowest direct gap. The detection of PL from $Ge_{1-x-y}Si_xSn_y$ alloys is important for the determination of their optical quality and, in the case of direct gap conditions, it represents the first step towards the realization of devices. Note, however, that the width of the

spectra is intrinsically related to the quality of the samples indicating that significant optimization in materials properties (reduced levels of defects and impurities) is needed. Furthermore, we find that the PL signal can be quenched by the presence of trace amounts of non-radiative recombination centers in otherwise structurally perfect samples. We have observed PL in several samples, but the material needs further improvement to display a strong signal on a routine basis.

RECENT ADVANCES MADE POSSIBLE BY Ge-Si-Sn BUFFERS ON Si(100)

a) Tensile-strained direct-gap elemental Ge via Si-Ge-Sn buffers: Tensile strained Ge is a topic of intense current research activity. The application of tensile strain to elemental Ge lowers its band gap to a range compatible with optical fiber communications, splits the valence band energy levels for enhanced mobility devices, and—for sufficiently high levels of strain—could lead to a direct gap material. Tensile-strained Ge has been obtained by growing Ge directly on Si substrates at high temperatures (800°C), and taking advantage of the smaller thermal expansion coefficient of Si to induce tensile strain in the Ge layer when the sample is quenched to room temperature values. This leads to maximum reported strains on the order of 0.25% in films as thick as 1μm, which is sufficient for some applications. However, it is apparent that this method does not allow for a precise control of the strain. Moreover, the resulting devices must incorporate a defective Si-Ge interface [10].

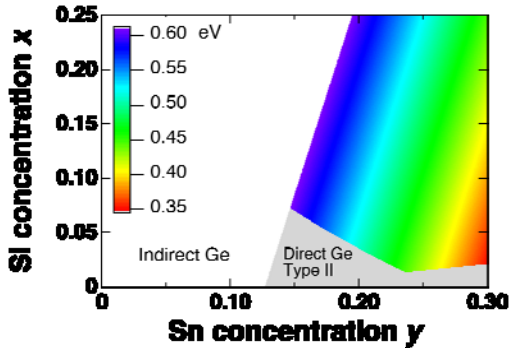

Figure 8. Band alignment for a $Ge/Ge_{1-x-y}Si_xSn_y$. It is assumed that the $Ge_{1-x-y}Si_xSn_y$ layer is relaxed, and that the Ge layer is strained to lattice-match $Ge_{1-x-y}Si_xSn_y$ (see Ref. 11)

The availability of GeSn buffers with a lattice constant larger than that of Ge promises to revolutionize the field of tensile-strained Ge. Based on critical thickness studies, strains exceeding 2% should be achievable, and this opens up intriguing new possibilities because the direct gap in Ge has a *stronger* dependence on tensile strain than the indirect gap. For strains approaching 2% the material becomes a direct gap semiconductor, with applications not only for detectors but also for lasers. To produce such strains GeSn buffers with Sn content above 10 at.% is needed as discussed below. Nevertheless as suggested in Fig. 8, the "near directness" of tensile strained Ge obtained on the unstrained GeSn buffers with only 4 % Sn content is still quite useful—despite the near parity in the energies of the L6 and Γ7 CB valleys-- because the 0.90 eV zone-center Γ7-LH vertical transition is rather strong and will dominate over the 0.76 eV L6-HH.

Tensile strained Ge grown on $Ge_{1-y}Sn_y$ buffers will have applications in high speed microelectronics due to the dramatic increase in mobility. However, for applications in detectors and light emitting devices, tensile-strained Ge layers should be surrounded (sandwiched) by a material with a higher band gap. One possibility is the ternary $Ge_{1-x-y}Si_xSn_y$ alloy, in which the presence of Si raises the value of the band gap. However, Si also reduces the lattice constant, and therefore the possibility of applying tensile strain on Ge is limited. We performed detailed calculations of $Ge/Ge_{1-x-y}Si_xSn_y$ heterostructures and found that it is possible to reach a

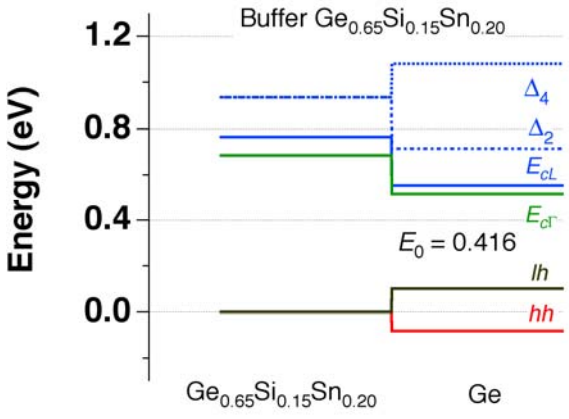

Figure 9. Calculated band diagram of a $Ge_{0.65}Si_{0.15}Sn_{0.20}$/Ge strained layer structure showing the indirect to direct cross over (green/blue). Note that holes are localized in light hole band (*lh*) due to tensile strain in Ge, which might lead to enhanced mobility.

compromise such that the Ge layer experiences enough tensile strain to become a direct gap material while the ternary $Ge_{1-x-y}Si_xSn_y$ still has a higher band gap [11]. Fig. 8 provides a graphical "phase diagram" of possible band alignments for this heterostructure. The figure shows that even for relatively modest Sn concentrations around 15%, it is possible to obtain direct-gap Ge with a band gap near 0.6 eV. This is because the band gap in the ternary increases very rapidly as a function of the Si concentration. Equally important, the concentrations can be chosen to produce a so-called Type-I band alignment, in which both electrons and holes are localized in the Ge layer. To illustrate a specific case, we present in Fig. 9 a result of our deformation potential calculation for a $Ge_{0.65}Si_{0.15}Sn_{0.20}$ buffer that gives Type I band alignment. As shown, the t-Ge layers have clear, direct band gap edge energy of 0.416 eV, corresponding to the 2.98 μm mid-infrared wavelength. This Ge is well suited for a 2.9 μm laser or sensor.

We have recently utilized $Ge_{1-y}Sn_y$ buffers to provide the tensile stress needed in routine and reproducible manner. Our approach is straightforward and suitable for large-scale integration [12]. Contrary to the thermal expansion approach yielding only 0.2% strains at 800°C, our growth proceeds at low temperatures (~350-400°C) compatible with CMOS processing. By growing Ge on $Ge_{1-y}Sn_y$ buffered Si, we have already obtained record high tensile stress on Ge by producing strains in the range of 0.4 %. The strained Ge films produced to date have utilize $Ge_{1-y}Sn_y$ buffers with y=0.02-0.040. High-quality, thermally stable, Ge layers have been deposited on these buffers at low temperatures 350-380°C. The strain state of the films is investigated by recording line scans and reciprocal space maps for the symmetric (004), and asymmetric (224) Bragg reflections. Figure 10 shows the (224) reciprocal space map

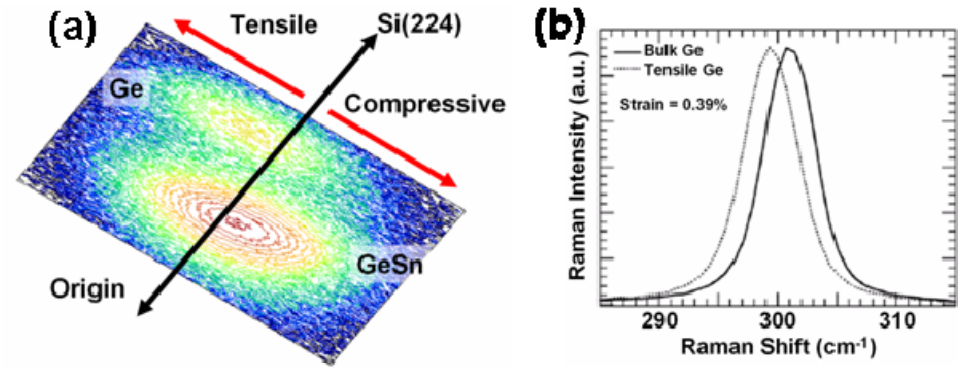

Figure 10: (a) XRD reciprocal space maps of the (224) reflections, showing the Ge epilayer and the $Ge_{0.96}Sn_{0.04}$ buffer relative to the Si substrate peak. The Ge peak falls above the relaxation line connecting the Si peaks and the origin, indicating tensile strain. (b) Raman spectrum comparing a tensile-

for a $Ge/Ge_{0.96}Sn_{0.04}$ structure with epilayer and buffer thicknesses of 60 nm and 200 nm, respectively. For the $Ge_{0.96}Sn_{0.04}$ buffer, the diffracted intensity peaks lie very close to the full relaxation line (black line in Fig. 10). The close vertical alignment of the Ge and GeSn (224) peaks indicates a fairly coherent heterostructure, while the considerable offset of the Ge peak with respect to the relaxation line implies a significant tensile strain. Using the measured vertical/horizontal lattice parameters and the calculated relaxed analog, a strain value of $\varepsilon_{||}$ = -0.35 ±0.02 %, is estimated for this sample. In Figure 10 the Raman spectrum from the tensile-strained Ge-film is shown. The Raman peak is clearly downshifted relative to the corresponding Raman peak in bulk Ge. From the observed Raman shift we deduce $\varepsilon_{||} = -0.39$ which is in good agreement with the X-ray analysis. Moreover, initial photoreflectance experiments on this sample confirm the downshift of the direct gap induced by the tensile strain.

A comprehensive study of Ge growth on Ge-Sn and Si-Ge-Sn buffers with variable composition is in progress. The objective is to tune the optical and electronics properties and produce a direct gap material based on this elemental semiconductor. Success could revolutionize the flourishing area of Si photonics**.** Based on critical thickness estimates and interpolation studies reported by Soref [13] strains approaching 2% should be achievable on unstrained $Ge_{1-y}Sn_y$ buffers for $y \sim 0.1$

b) Ge or SiGe grown on Si-Ge-Sn buffers for quantum cascade applications: The ternary alloy SiGeSn offers the unusual and important benefit of providing independent adjustment (via variation of x and y) of the alloy's lattice parameter and bandgap. We have mapped out this lattice and gap space. In addition, we have calculated the band structure of lattice matched Ge/GeSiSn multi quantum well structures that are suitable for a quantum cascade laser applications. Two MQW results are presented in Fig. 11. Here we see, that although the Ge is indirect, the 0.24 eV CB offset in (B) is quite useful for an n-type QCL. In addition to Ge/SiGeSn, there are strained-layer MQWs that will work for QCLs. These include GeSn/GeSiSn QW stacks and GeSi/GeSn MQWs. We have grown Ge rich $Ge_{0.80}Si_{0.20}$ alternating with $Ge_{0.98}Sn_{0.02}$ and we find experimentally that the relaxed lattice constant of the SiGe epilayer and the lattice constant of the GeSn buffer shift towards a common value to minimize the strain energy. Thus, as discussed here, we have good prospects for obtaining QCLs structures. As a footnote to Fig. 11 above, we note that the indirect (but nearly direct) Ge layers will probably give a strong electroabsorption modulation (the quantum confined Stark effect) in the midwave and longwave infrared [14].

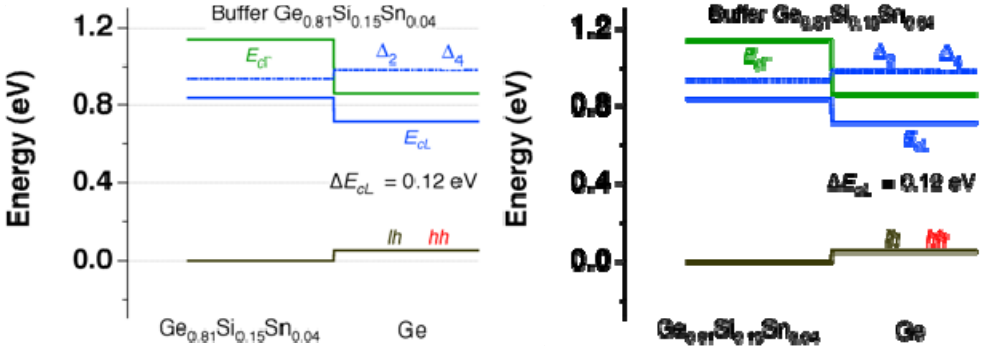

Figure 11. Band edge diagrams for lattice-matched, unstrained SiGeSn/Ge heterostructures in which electrons and holes are confined in the Ge layer (Type I). Two different buffer compositions were investigated.

(c) SiSn alloys on GeSn: New materials with direct band gaps in the 1.3-1.55 μm range: An interesting example of a group IV system with potential applications in the communication wavelength range is the SiSn alloy, which was recently synthesized (for the first time by CVD) in our lab [15]. This material was grown on GeSn buffered Si via reactions of SnD_4 and $SiH_3SiH_2SiH_3$ at 275 ^oC. Compositions of 20-35 % Sn have been grown and characterized by XRD, XTEM and RBS. The data show that the films grow lattice matched to the buffer layers. Raman reveals for the first time the presence of Si-Sn bonds and the Raman shifts of the Si-Sn and Si-Si modes are consistent with the RBS composition. The key to the successful synthesis is the use of highly reactive silane sources that furnish Si atoms at low temperatures, and the use of lattice matched GeSn buffers that promote growth of metastable phases via an epitaxialy driven "compositional pinning" mechanism. The unprecedented low growth temperature is made possible by the highly reactive SiH_2 groups in $SiH_3SiH_2SiH_3$. We conducted simulations of the electronic and structural properties of a series of random SiSn alloys for Sn concentrations up to 50% using density functional theory DFT/LDA. These calculations predict that a transition from indirect to direct is likely for ~25-40% Sn. For a nominal composition of about 32 % Sn the direct gap is about ~ 0.9 eV based on corrected LDA values. At 20 % Sn the direct and indirect gaps are 0.93 eV and 0.90 eV respectively. The close values indicate that the gap can potentially become direct at compositions close to 25 % with a corresponding wavelength of 1.33 μm.
We have been able to accurately predict the structural properties of the Si-Sn systems and the deviations of the lattice parameters from Vegard's behavior are found to be negligible. Therefore we can use well established $Ge_{1-y}Sn_y$ buffers with y= 0.02, 0.07 and 0.12 to grow lattice matched $Si_{1-z}Sn_z$ with z = 0.25, 0.28 and 0.35 respectively.

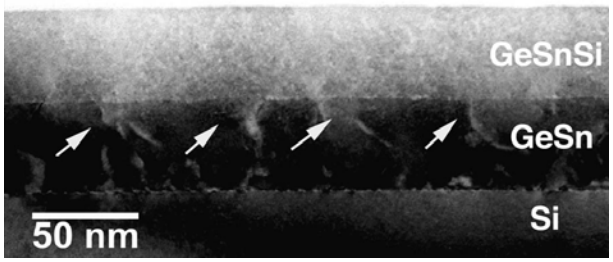

Figure 12. XTEM of highly mismatched GeSiSn/GeSn/Si heterostructure. The top layer is defect free and displays a flat surface. The bulk of the defects are concentrated in the buffer layer. Defects originating at the GeSiSn/GeSn interface appear to be absorbed by the "softer" GeSn buffer layer as indicated by arrows (see Ref. 3).

b) III-V and II-VI compound integration with Si: Above we discuss that GeSn possess a set of unique microstructural and morphological properties which make them imminently suitable as buffers for integration of semiconductors with Si. Recently we have shown that these properties also extend to GeSiSn based buffers. The latter however possess additional benefits such as lattice constants above and below that of Ge and tunable thermal expansion behavior between the three elements. Also like GeSn the SiGeSn buffers provide a cushioning effect that can absorb defects caused by the differential strain imposed in highly mismatched heteroepitaxy [3]. The latter concept is demonstrated in Fig. 12 for a SiGeSn/GeSn structure. The lattice constants for the two layers are 5.58 and 5.71 Å, respectively. The top layer is virtually defect free while the GeSn buffer contains significant levels of defects. A number of these defects originate at the SiGeSn/GeSn interface and show the propensity to propagate downward into the "softer" GeSn film. This is unexpected, since the same GeSn material "as grown" on Si is free of threading defects. The only plausible

explanation is that the GeSn buffer possesses a unique ability to absorb stress from a mismatched overlayer. GeSiSn alloys are attractive as buffer layers because they allow independent tuning of the lattice constant and thermal expansion coefficient.

The main application of this concept is the minimization of the thermal expansion mismatch between the buffer layer and the Si substrate. A good example is the growth of GaAs on graded GeSi/Ge buffer layers. The very large thermal expansion mismatch between Ge and Si lead to cracking of the films. The critical thickness, t_c, for crack formation is given by $E_s(1-\nu)/(G(1+\nu)f^2)$ where E_s is the energy for crack formation[16], ν the Poisson ratio, G the shear modulus, and f the strain due to difference in thermal expansion coefficients, $f = (a_{film}-a_{substrate})\Delta T$. GeSiSn can provide a lattice constant identical to Ge but with a much smaller thermal expansion mismatch. In the extreme case of $Si_{0.8}Sn_{0.2}$, the thermal expansion mismatch is reduced by a factor of 5, so that the critical thickness increases by a factor of 25. Using a more realistic composition of $Ge_{0.5}Si_{0.4}Sn_{0.1}$ the thermal expansion mismatch is reduced by a factor of 1.6, which more than doubles the critical thickness for crack formation. Thus the GeSiSn system provides entirely new pathways for integration with Si through simultaneous lattice and thermal matching.

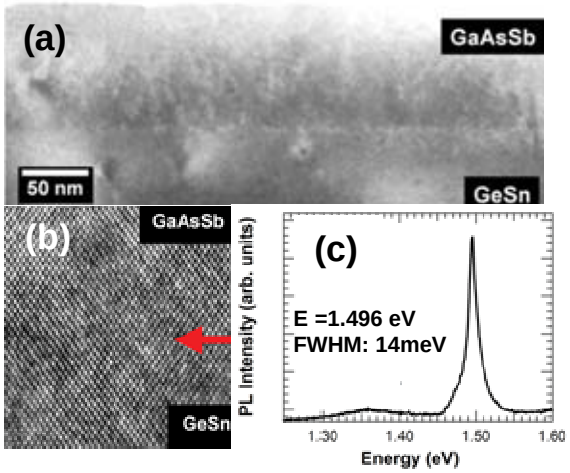

Figure 13. (a) Bright field image of a lattice matched GaAsSb/$Ge_{0.92}Sn_{0.08}$ layer. (b) Corresponding high resolution image of interface. (c) PL from a InGaAs/GeSn sample. Note the peak width is comparable to that obtained from InGaAs grown on bulk GaAs (Ref. 15).

The utility of these buffer systems to integrate III-V materials and devices with Si, has prompted us to undertake extensive growth studies via MOCVD. These have produced GaAs/AlGaAs quantum wells, III- antimonides and strain-engineered $In_xGa_{1-x}As$ and $GaAs_{1-x}Sb_x$ alloys on $Ge_{1-y}Sn_y$ (y= 0.02-0.08) buffers (Fig. 13). Their optical properties (PL) and microstructure in most cases compare well with those measured in fully relaxed micrometer-thick layers grown on bulk GaAs. This indicates that our approach provides a viable technology for the growth of high quality III-Vs on Si substrates [16].

CONCLUDING REMARKS

The SiGeSn system provides a novel approach to extend the utility of pure Ge in IR emission, detection and sensing technologies. SiGeSn buffers with lattice constants larger those of Ge can be used to develop a practical route to type I Ge/SiGeSn strained-layer heterostructures possessing tunable, direct Ge bandgaps. The light emission from these systems should be strong due to the direct nature of the optical transition and the spatial confinement of electrons and holes within the same strained Ge layer. This together with our very recent demonstration of luminescence in the related Si-Ge-Sn materials represents a critical milestone in the flourishing field of Si photonics and it is likely to lead to significant breakthroughs in device design and fabrication. This Si-Ge-Sn class of materials including GeSn, SiGeSn, SiGe, Ge (strained) and SiSn collectively span all of the technologically relevant direct and indirect

Fig. 12. Bright field image of an $Ge_{0.98}Sn_{0.02}$

gaps in the IR, leading to the practical realization of lasers, high speed modulators (~ GHz) and sensitive photodetectors based entirely on group IV materials. This concept represents a new paradigm in the integration of Si based electronic with optical components on a single chip. Although our work to date represents a significant initial effort, it also lays the foundation for the systematic development of "silicon photonics" a new area of material science and engineering.

ACKNOWLEDGMENTS

The authors wish to thank the Air Force Office of Scientific Research (Dr. Gernot Pomrenke, Program Manager) for sponsorship of this research, AFOSR MURI, FA9550-06-01-0442. The XRD equipment use in this study was purchased by a grant from the National Science Foundation the NSF (DMR-0526604).

REFERENCES

1. M. R. Bauer, J. Taraci, J. Tolle A.V.G Chizmeshya, S. Zollner, J. Menendez, D. J. Smith, J. Kouvetakis, *Appl. Phys. Lett.* **81,** 2992-2994 (2002).
2. J. Kouvetakis, J. Menendez, A.V.G Chizmeshya, *Annual Reviews of Materials Research* **36**, 497-554 (2006).
3. R. Roucka, J. Tolle, C. Cook, V.J. Costa, A.V.G Chizmeshya, J. Menendez, S. Zollner, J. Kouvetakis, *Appl. Phys. Lett.* **86(19),** 191912/1-3 (2005).
4. M. R. Bauer, J. Kouvetakis, D.J. Smith and J. Menendez, *Solid State Commun.* **127**, 355-359, (2003).
5. V. D'Costa, C. Cook, A.G. Birdwell, C. A. Littler, S. Zollner J. Kouvetakis, J. Menendez, *Phys. Rev.* B **73**, 125207(1-16) (2006).
6. C. Ritter, J. Tolle, V. D'Costa, J. Menendez, A.V.G. Chizmeshya, J. Kouvetakis, *Chem. Mater.* **18,** 6266-6277 (2006).
7. P. Aella, C. Cook, J. Tolle, S. Zollner, A.V.G. Chizmeshya, J. Kouvetakis, *Appl. Phys. Lett.* **84**, 888-890, (2004).
8. J. Tolle, R. Roucka, V. D'Costa, J. Menendez, A. Chizmeshya, J. Kouvetakis, *Appl. Phys. Lett.* **88(25),** 252112**,** (2006).
9. V. R. D'Costa, Candi S. Cook, J. Menéndez, J. Tolle, J. Kouvetakis, S. Zollner, *Solid State Commun.* **138(6),** 309 (2006).
10. Y. Ishikawa, K. Wada, D. D. Cannon, J. Liu, H.-C. Luan, L. C. Kimerling, *Appl. Phys. Lett.* **82**, 2044 (2003).
11. J. Menendez, J. Kouvetakis, *Appl. Phys. Lett.* **85(7)** 1175 (2004)**.**
12. Y-Y Fang, J. Tolle, V. D'Costa, J. Menendez, J. Kouvetakis *Appl. Phys. Lett.* **90,** 061915 (2007).
13. R. A. Soref, L. Friedman, *Superlattices and Microstructures* **14 (213)**, 189 (1993).
14. R. A. Soref, J. Kouvetakis, J. Menendez, *US Patent* 6,897,471 (2005)**.**
15. J. Tolle, V. D'Costa, A.V.G. Chizmeshya, C-W. Hu, I.S.T Tsong, Jose Menendez, J. Kouvetakis *Appl. Phys. Lett.* **89,** 231924 (2006)..
16. R. Roucka, J. Tolle, V. D'Costa, J. Menendez, J. Kouvetakis *J. Appl. Phys.* **101**, 013518 (2007).